

# PROPEL: Probabilistic Parametric Regression Loss for Convolutional Neural Networks

Muhammad Asad <sup>\*1,2</sup>, Rilwan Basaru<sup>2</sup>, S M Masudur Rahman Al Arif<sup>2,3</sup>, and Greg Slabaugh<sup>2</sup>

<sup>1</sup>Imagination Technologies, <sup>2</sup>City, University of London, <sup>3</sup>Netherlands Cancer Institute

## Abstract

Recently, Convolutional Neural Networks (CNNs) have dominated the field of computer vision. Their widespread success has been attributed to their representation learning capabilities. For classification tasks, CNNs have widely employed probabilistic output and have shown the significance of providing additional confidence for predictions. However, such probabilistic methodologies are not widely applicable for addressing regression problems using CNNs, as regression involves learning unconstrained continuous and, in many cases, multi-variate target variables. We propose a PRObabilistic Parametric rEgression Loss (PROPEL) that enables probabilistic regression using CNNs. PROPEL is fully differentiable and, hence, can be easily incorporated for end-to-end training of existing regressive CNN architectures. The proposed method is flexible as it learns complex unconstrained probabilities while being generalizable to higher dimensional multi-variate regression problems. We utilize a PROPEL-based CNN to address the problem of learning hand and head orientation from uncalibrated color images. Comprehensive experimental validation and comparisons with existing CNN regression loss functions are provided. Our experimental results indicate that PROPEL significantly improves the performance of a CNN, while reducing model parameters by  $10\times$  as compared to the existing state-of-the-art.

## 1. Introduction

Convolutional Neural Networks (CNNs) are enabling major advancements in a range of machine learning problems [14, 16, 19, 21, 27, 28, 32]. Their success has been widely reflected by their application in a number of domains, most notably for image classification [16, 19, 28] and segmentation problems [14, 15, 27, 32], where they

<sup>\*</sup>This work was done when Muhammad Asad was with City, University of London.

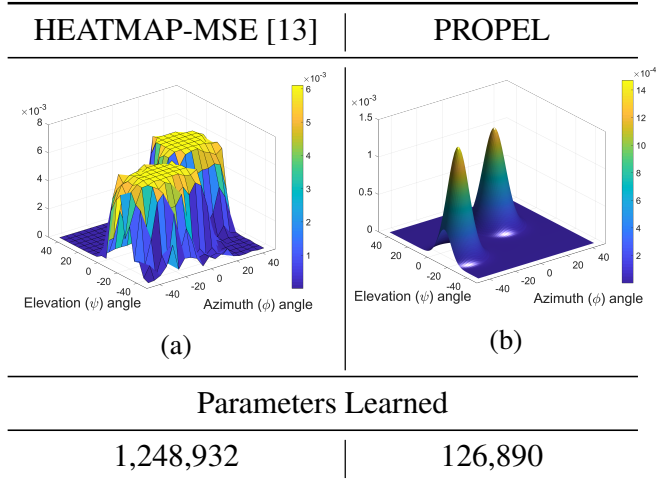


Figure 1: Comparison of predictions from (a) HEATMAP-MSE [13] and (b) PROPEL (proposed). PROPEL learns parametric probability distributions requiring  $10\times$  fewer model parameters, while resulting in more confident predicted distributions. The predictions from PROPEL are parameters for a probability distribution (shown as a continuous distribution in (b)). In contrast, (a) directly learns a non-parametric distribution of size  $20 \times 20$ .

have outperformed conventional machine learning methods. The existing state-of-the-art for CNN-based classification and segmentation benefits from probability distributions for target class prediction [16, 19, 27, 28, 32]. These distributions provide additional confidence information that can be useful to determine the level of uncertainty in a given prediction. They can also help resolve ambiguous model predictions [5]. Furthermore, for complex learning problems where dividing a given learning task into smaller subtasks can help, probabilistic models provide a flexible framework for combining the predictions from multiple models [5, 12, 18]. Moreover, the probabilistic predictions enable incorporation of priors using Bayes' rule for applications where prior class distributions are known [6].

Despite widespread application of CNNs for probabilistic classification, little emphasis has been made for unconstrained probabilistic regression. Regression using a CNN has been restricted to target space learning using a Mean Squared Error (MSE) that does not provide a probabilistic output [10, 23]. In some existing methods, non-parametric probabilistic target variables are learned using MSE in the form of probability heatmaps [7, 13, 31]. These methods make assumptions that the target continuous variables can be constrained within a specified domain which is useful for generating heatmap distributions. This limits the application of such methods to only a specific domain, where they are unable to generalize well for unconstrained multi-variate regression problems. Moreover, non-parametric probabilities require the output layer to represent a significantly large dimensional heatmap. This contributes to the complexity of the model, requiring larger number of parameters to be learned with significantly increased learning time and training data.

We address the existing issues with CNN-based regression by proposing a novel PRObabilistic Parametric rEgression Loss (PROPEL) that enables a CNN model to output parametric regression probabilities. This is achieved by using a loss function that models the CNN output as a parameterized Mixture of Gaussians in the target space. PROPEL is fully differentiable with a novel analytic closed-form solution to integrals, allowing it to be used for end-to-end training of existing CNN regressive architectures. Moreover, PROPEL is generalizable for modeling different levels of complexity within prediction probabilities as well as the number of dimensions for addressing multi-variate regression problems. As the output is parameterized by a Mixture of Gaussians, the proposed layer requires fewer number of output parameters as compared to previously used probability heatmaps. In this paper, PROPEL is used to address the problem of color image-based hand and head orientation regression [5, 11]. We show that PROPEL-based CNN outperforms state-of-the-art regression losses. Moreover, it enables the model to generalize better and resolve ambiguities in a dataset, while using  $10\times$  fewer model parameters as compared to the existing state-of-the-art (as shown in Fig. 1).

**Our Contributions.** The main contributions of this paper are:

- To the best of our knowledge, we are the first to propose PROPEL, a fully differentiable loss layer for enabling unconstrained probabilistic parametric regression using CNNs. A novel derivation is provided for the proposed loss using Mixture of Gaussians distribution;
- We present a generalizable framework that handles any number of target dimensions and has the ability to model complex multimodal probabilities with additional Gaussians in the mixture;
- We show that the proposed PROPEL can help address ambiguities in predictions by enabling a model to output expressive predictions in the form of parametric probabilities;
- We provide comprehensive experimental validation and comparisons with existing methodologies and report that the proposed loss outperforms existing state-of-the-art by a large margin, while using  $10\times$  fewer model parameters.

## 2. Related Work

**Probabilistic Regression using CNN.** Previous work has mostly been focused on exploring non-parametric probabilistic regression for CNNs [2, 7, 13, 25, 30, 31]. These methods first generate the ground truth probability heatmap distributions in the target space. A CNN is then trained using a Mean Squared Error (MSE) loss to learn the mapping of input images onto the heatmaps. Tompson et al. [31] generated and employed single-view heatmaps for hand joints localization using depth images as input. Ge et al. [13] extended [31] to use multi-view CNN, where heatmaps from three projections of depth images were used. Three separate CNNs were trained to infer the heatmaps of different joint locations in each projection. Similar methods were also proposed for human pose estimation using a CNN [7, 25]. Recently, Al Arif et al. [2] proposed to learn heatmap distributions of cervical vertebrae locations by utilizing the Bhattacharyya coefficient (BC). The use of BC resulted in better accuracy as it measured a probabilistic loss between two heatmap probability distributions. Pathak et al. [24] employed probabilistic interpretation of Euclidean loss to enforce a set of known constraints on the model outputs.

Lathuilière et al. [20] jointly learned both a CNN model, for representation learning, and a Gaussian mixture of linear inverse regressions by utilizing a modified Expectation Maximization (EM) algorithm. Crucially, this approach utilized a pre-trained CNN model; and EM is known to suffer from sensitivity to initialization. Similar to PROPEL, this approach enabled probabilistic regression using CNNs. The method, however, required a carefully designed initialization, that included a pre-trained CNN and clustering of data. Moreover, their initialization was based on the assumption that the data can be easily clustered with known number of clusters. In contrast, our proposed PROPEL is a fully differentiable loss that enables end-to-end training of a CNN model. As PROPEL has a closed-form solution, it can be easily incorporated within existing CNN architectures, and can learn models from scratch using backpropagation. As

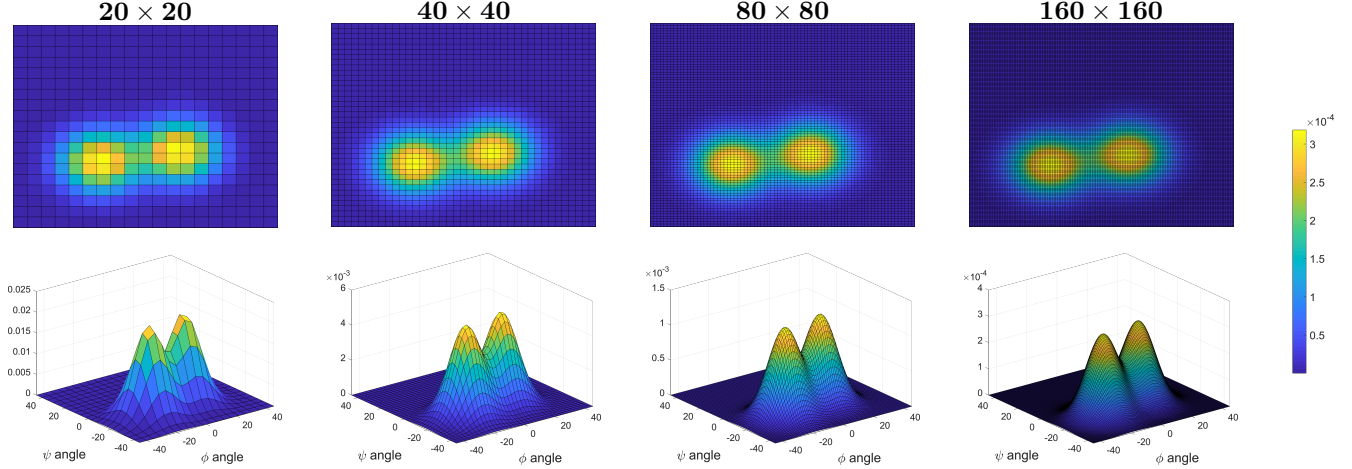


Figure 2: Heatmap size versus resolution of the probability density function (PDF) shows that a smaller size results in lower accuracy, while larger size contributes towards better approximation of the PDF. The majority of the heatmap distribution consists of values close to zero, which results in under-utilization of the allocated model parameters.

indicated by our experimental validation, PROPEL generalizes well from smaller dataset, while also helping to significantly reduce the model parameters.

Non-parametric heatmap distributions only work in problems where target space can be fully defined within a finite domain, such as hand or body joint localization [7, 13, 25, 31]. While such assumptions prove useful for introducing and benefiting from the probabilistic regression in CNNs, they limit generalization of such methods and their application to other regression problems. Furthermore, the parameters required to learn a non-parametric probability distribution are much higher as such methods directly learn the distributions. Achieving high accuracy from these methods often requires high-resolution heatmap distributions, resulting in higher number of model parameters (see Fig. 2 and Fig. 3). In addition, the majority of a non-parametric heatmap distribution contains values close to zero. This results in under-utilization of the allocated model parameters as most of the output parameters are set to zero during inference. Learning higher dimensional target variables also results in rapid increase in model parameters, where existing methods split the problem into learning multiple 2D heatmaps [7, 13, 31].

The proposed PROPEL method addresses the existing limitations of non-parametric probabilistic regression by utilizing a parametric loss function that is fully differentiable. In addition to significantly reducing model parameters, PROPEL does not require the target space to be constrained. Furthermore, the proposed solution is generalizable in terms of target variable dimension and prediction probability complexity. As a result, PROPEL can be easily applied to existing regression problems with any number of target dimensions without constraining the

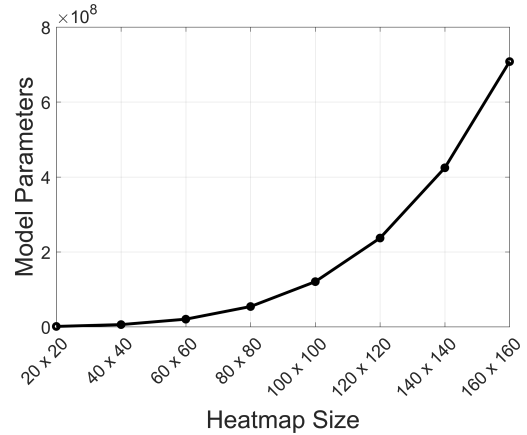


Figure 3: Heatmap size versus number of required model parameters for CNN architecture in Fig. 5, where only the number of neurons within the fully connected layers Fc1 and Fc2 are changed to match the size of a given heatmap distribution. The number of model parameters increases exponentially with increased heatmap size. In contrast, PROPEL uses parameterized probabilities where modeling complex distributions only require adding more Gaussians ( $I$ ) to the Mixture of Gaussians. This is linearly related by  $d = 2 \times n \times I$  to the model parameters, and hence requires significantly less model parameters.

learned probabilities. We provide PROPEL along with its partial derivatives, which enables its application for end-to-end training of existing CNN architectures using backpropagation.

**Orientation Estimation.** In this paper, we demonstrate the

ability of the proposed method to learn and outperform existing methods for image-based hand and head orientation regression.

Image-based hand orientation regression has only been applied in [3, 4, 5]. [3] utilized two single-variate Random Forest (RF) regressors based on an assumption that the orientation angles vary independently. This method, evaluated on a subset of hand orientation angles, showed the significance of inferring hand orientations from 2D uncalibrated color images. Later, [4] used a multi-layered Random Forest regression method that utilized multi-variate regressors to regress the orientation angles together. Similarly, [5] presented a staged probabilistic regressor, which learned multiple expert Random Forests in stages and employed a multi-layered regressor [5]. These image-based hand orientation regression methods do not require camera calibration which renders them suitable for a wider array of applications across different devices. The datasets used for training come from multiple people, which enables these methods to naturally handle person-to-person hand variations.

All existing image-based hand orientation regression methods utilize hand-crafted features. In this paper, we show that the task of hand orientation regression can benefit from the representation learning capability of CNN. Utilizing MSE, we show that a CNN model, without any probabilistic output, can significantly outperform existing methods that use hand-crafted features. We use this model as baseline for our experimental validation and demonstrate that the proposed probabilistic parametric regression loss can outperform existing regression loss functions for CNNs. This is particularly due to PROPEL’s ability to handle ambiguity in hand orientation datasets by utilizing probabilistic parametric distributions to comprehensively represent the predictions.

A number of existing methods address head orientation regression using color images [8, 1, 22, 20]. Drouard et al. [8] proposed Gaussian mixture of locally-linear mapping model. This method learned the mapping of HOG-based features onto head orientation, additionally providing probabilistic output. Later, Lathuilière et al. [20] improved [8] by utilizing a pre-trained CNN for feature extraction. This method, however, relied on a modified EM algorithm for fine-tuning CNN and learning the mapping of features onto target head orientations. CNN-based head orientation regressors were proposed in [1, 22]. Both methods learned using MSE loss, where [22] utilized an additional synthetic dataset for improving the model. In our experimental validation section, we compare against these existing methods and show that the proposed PROPEL can outperform existing state-of-the-art for head orientation estimation that utilize CNNs.

### 3. Method

We now describe the details of our proposed PRObabilistic Parametric rEgression Loss (PROPEL). First, we introduce the loss function and the corresponding parametric probabilities. This is followed by the derivation of a novel analytic closed-form solution to the integrals within our loss function that are required for computing the loss over an unconstrained real space. Lastly, we provide details of the partial derivatives of our loss function which allows PROPEL to be integrated with existing CNN architectures using backpropagation.

#### 3.1. Probabilistic Parametric Regression Loss

We expand on [26] by introducing a regression loss function for learning a CNN model. The existing measures, such as Bhattacharyya coefficient (BC) and Kullback-Leibler (KL) divergence, are tractable when distributions are *unimodal*, i.e. each consisting of a single Gaussian. However, it is well-known that these metrics between *multimodal* Mixture of Gaussians have no analytic solution [17, 9] and at best, one must resort to approximation. However, to address modelling of complex multimodal probabilistic distributions, and handling ambiguous predictions (see Fig. 7), Mixture of Gaussians are essential. This motivates the use of metric from [26] for proposing PROPEL, as this metric has an analytic closed-form solution when distributions are Mixture of Gaussians. We show, for the first time in this paper, how to analytically address neural network regression using a Mixture of Gaussians loss. PROPEL is fully differentiable, enabling us to determine both the loss and gradient of a model distribution  $P_m$  with respect to a ground truth (GT) distribution  $P_{gt}$ . Let  $\mathbf{x} = \{x_1, x_2, \dots, x_n\}^T \in \mathbb{R}^n$  define the target prediction space with  $n$  dimensions, the proposed loss can be defined for  $\mathbf{x}$  as:

$$L = -\log \left[ \frac{2 \int P_{gt} P_m d\mathbf{x}}{\int (P_{gt}^2 + P_m^2) d\mathbf{x}} \right], \quad (1)$$

where  $P_{gt}$  is the  $n$ -dimensional GT PDF defined by a Gaussian distribution as:

$$P_{gt}^k = \frac{e^{-\frac{1}{2} \left[ \frac{(x_1 - \mu_{x_{1k}})^2}{\sigma_{x_{1k}}} + \dots + \frac{(x_n - \mu_{x_{nk}})^2}{\sigma_{x_{nk}}} \right]}}{(\sqrt{2\pi})^n \sqrt{\sigma_{x_{1k}} \dots \sigma_{x_{nk}}}}, \quad (2)$$

where  $k$  represents a sample selected from a given dataset,  $\mu_{x_{1k}}, \mu_{x_{2k}}, \dots, \mu_{x_{nk}}$  are the GT observations and  $\sigma_{\mu_{x_{1k}}}, \sigma_{\mu_{x_{2k}}}, \dots, \sigma_{\mu_{x_{nk}}}$  are the GT variances associated with  $P_{gt}$ . The numerator in Equation 1 evaluates similarity between a GT PDF  $P_{gt}$  and a model PDF  $P_m$ , whereas the denominator eliminates bias towards specific shapes of probability distributions.

In addition to the GT distribution  $P_{gt}$ , PROPEL requires a model distribution  $P_m$ . The choice of  $P_m$  determines the ability of a trained model to handle complex variations in target space for a given dataset. We recognize that any

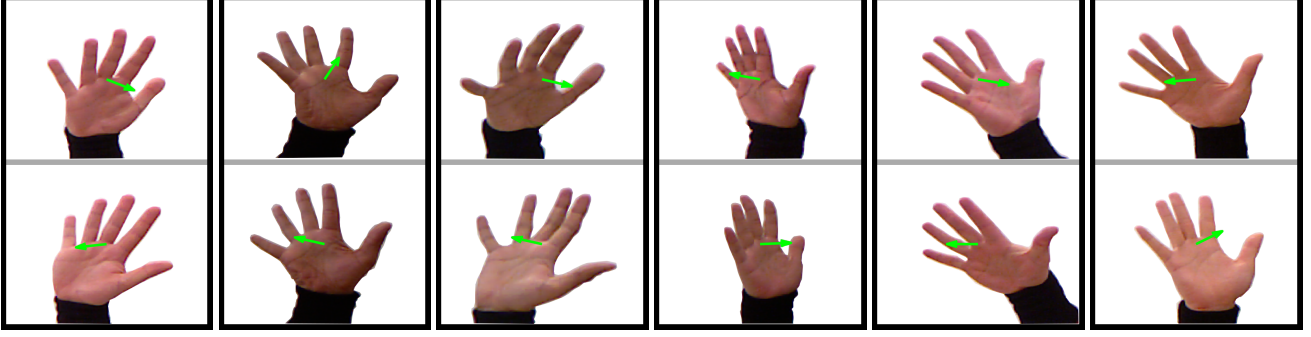


Figure 4: Symmetry problem due to depth ambiguity in hand orientation dataset shows image pairs with different orientations (shown with green arrows) but similar hand shapes. Such ambiguities motivate the use of multimodal probability distributions as the model distribution  $P_m$  in PROPEL.

parametric PDF can be utilized as the model distribution. Our work is motivated by a limitation of existing regression techniques for addressing ambiguity within a given dataset. Consider the problem of learning hand orientations from uncalibrated color images. As noted in existing literature [4] and shown in Fig. 4, the absence of depth information results in ambiguity, where multiple symmetrically opposite hand orientations have similar color images. In cases where such ambiguities exist, a unimodal probabilistic distribution proves insufficient (the same is true for probabilistic interpretation of MSE). In contrast, utilizing a multimodal distribution enables the regressor to address such ambiguities by learning to infer multiple hypotheses [4, 5]. In this work, we use a Mixture of Gaussians as the model distribution  $P_m$  because it facilitates in keeping our derivations simple, while also enabling us to model complex multimodal distributions. Moreover, in comparison to existing state-of-the-art which uses non-parametric heatmaps, a Mixture of Gaussians only requires a fraction of parameters (means and variances) for modeling a distribution. This reduces the number of model parameters as well as the overall complexity of a CNN model. The number of Gaussians in the Mixture of Gaussians also enable us to learn complex probability distributions that can handle ambiguous predictions, resulting in better accuracy while keeping the derivation consistent. For a target space with  $n$  dimensions,  $P_m$  is defined as:

$$P_m = \frac{1}{I} \sum_{i=1}^I P_i = \frac{1}{I} \sum_{i=1}^I \frac{e^{-\frac{1}{2} \left[ \frac{(x_1 - \mu_{x_{1i}})^2}{\sigma_{x_{1i}}} + \dots + \frac{(x_n - \mu_{x_{ni}})^2}{\sigma_{x_{ni}}} \right]}}{(\sqrt{2\pi})^n \sqrt{\sigma_{x_{1i}} \dots \sigma_{x_{ni}}}}, \quad (3)$$

where  $P_i$  represents an individual  $i^{th}$  Gaussian within a Mixture of Gaussians,  $\mu_{x_{1i}} \dots \mu_{x_{ni}}$  and  $\sigma_{x_{1i}} \dots \sigma_{x_{ni}}$  are model parameters inferred as the output of a CNN network and  $I$  is the total number of Gaussians in  $P_m$ . Note that the weights for each Gaussian in the mixture are fixed to  $\frac{1}{I}$  in our method. Our model distribution does not include covariances as in our experimental validation we found variances to be sufficient for outperforming the state-of-the-art meth-

ods. The next section provides a novel analytic closed-form solution of the loss function  $L$  such that we can evaluate integrals over the continuous domain  $-\infty$  to  $+\infty$ .

### 3.2. Analytic Solution to Integrals

Given the loss function  $L$ , the model PDF  $P_m$  and GT PDF  $P_{gt}$ , we can substitute these PDFs in Equation 1 and simplify.

$$L = -\log \left[ \frac{2 \int P_{gt} P_m d\mathbf{x}}{\int (P_{gt}^2 + P_m^2) d\mathbf{x}} \right], \quad (4)$$

$$= -\log \left[ 2 \int P_{gt} P_m d\mathbf{x} \right] + \log \left[ \int P_{gt}^2 d\mathbf{x} + \int P_m^2 d\mathbf{x} \right], \quad (5)$$

$$= -\log \left[ \underbrace{\frac{2}{I} \sum_{i=1}^I G(P_{gt}, P_i)}_{T1} \right] + \log \left[ \underbrace{H(P_{gt}) + \frac{1}{I^2} \sum_{i=1}^I H(P_i) + \frac{2}{I^2} \sum_{i < j} G(P_i, P_j)}_{T2} \right], \quad (6)$$

where the functions  $G(P_i, P_j)$  and  $H(P_i)$  represent the analytic solutions to the integrals  $\int P_i P_j d\mathbf{x}$  and  $\int P_i^2 d\mathbf{x}$ , respectively.  $P_i$  and  $P_j$  are two multi-variate Gaussian distributions. Both  $G(\cdot)$  and  $H(\cdot)$  are defined as follows<sup>1</sup>:

$$G(P_i, P_j) = \int P_i P_j d\mathbf{x}, \quad (7)$$

$$= \frac{e^{\left[ \frac{2\mu_{x_{1i}}\mu_{x_{1j}} - \mu_{x_{1i}}^2 - \mu_{x_{1j}}^2}{2(\sigma_{x_{1i}} + \sigma_{x_{1j}})} + \dots + \frac{2\mu_{x_{ni}}\mu_{x_{nj}} - \mu_{x_{ni}}^2 - \mu_{x_{nj}}^2}{2(\sigma_{x_{ni}} + \sigma_{x_{nj}})} \right]}}{(\sqrt{2\pi})^n \sqrt{(\sigma_{x_{1i}} + \sigma_{x_{1j}}) \dots (\sigma_{x_{ni}} + \sigma_{x_{nj}})}}. \quad (8)$$

$$H(P_i) = \int P_i^2 d\mathbf{x} = \frac{1}{(2\sqrt{\pi})^n \sqrt{\sigma_{x_{1i}} \dots \sigma_{x_{ni}}}}. \quad (9)$$

<sup>1</sup>Complete derivation of integrals in functions  $G(\cdot)$  and  $H(\cdot)$  is provided in the accompanying Appendix A.



Next, we show how the loss  $L$  from Equation 6 can be used alongside existing CNN architectures that use back-propagation algorithm for training.

### 3.3. Optimization

In this section we present the partial derivatives of  $L$  with respect to model parameters  $\mu_{x_{ni}}, \sigma_{x_{ni}}$ . These can be used for end-to-end training of a CNN using backpropagation. We can derive partial derivatives of  $L$  as:

$$\frac{\partial L}{\partial \mu_{x_{ni}}} = -\frac{1}{T1} \left[ \frac{\partial G(P_{gt}, P_i)}{\partial \mu_{x_{ni}}} \right] + \frac{1}{T2} \left[ \frac{2}{I^2} \sum_{i < j} \frac{\partial G(P_i, P_j)}{\partial \mu_{x_{ni}}} \right], \quad (10)$$

$$\frac{\partial L}{\partial \sigma_{x_{ni}}} = -\frac{1}{T1} \left[ \frac{\partial G(P_{gt}, P_i)}{\partial \sigma_{x_{ni}}} \right] + \frac{1}{T2} \left[ \frac{1}{I^2} \frac{\partial H(P_i)}{\partial \sigma_{x_{ni}}} + \frac{2}{I^2} \sum_{i < j} \frac{\partial G(P_i, P_j)}{\partial \sigma_{x_{ni}}} \right]. \quad (11)$$

The partial derivatives  $\frac{\partial G(P_i, P_j)}{\partial \mu_{x_{ni}}}$ ,  $\frac{\partial G(P_i, P_j)}{\partial \sigma_{x_{ni}}}$  and  $\frac{\partial H(P_i)}{\partial \sigma_{x_{ni}}}$  are defined as:

$$\frac{\partial G(P_i, P_j)}{\partial \mu_{x_{ni}}} = \frac{(\mu_{x_{nj}} - \mu_{x_{ni}})}{(\sigma_{x_{ni}} + \sigma_{x_{nj}})} G(P_i, P_j), \quad (12)$$

$$\frac{\partial G(P_i, P_j)}{\partial \sigma_{x_{ni}}} = [\cdot] G(P_i, P_j), \text{ where,} \quad (13)$$

$$[\cdot] = \frac{(\mu_{x_{ni}}^2 + \mu_{x_{nj}}^2 - 2\mu_{x_{ni}}\mu_{x_{nj}} - \sigma_{x_{ni}} - \sigma_{x_{nj}})}{2(\sigma_{x_{ni}} + \sigma_{x_{nj}})^2}, \quad (14)$$

$$\frac{\partial H(P_i)}{\partial \sigma_{x_{ni}}} = \frac{-1}{2\sigma_{x_{ni}}} H(P_i). \quad (15)$$

At each training iteration, the proposed PROPEL loss layer computes the loss in the forward pass using Equation 6 on the output from the CNN model. For the backward pass, the partial derivatives are used along with the GT distribution to backpropagate the error and optimize the parameters using RMSProp [29].

## 4. Experimental Validation

We perform experimental validation of PROPEL by addressing image-based hand and head orientation regression problems. Given a dataset  $\mathcal{U} = \{(\mathbf{C}_k, \mathbf{o}_k)\}_{k=1}^K$  with  $K$  uncalibrated color images  $\mathbf{C}_k$  of hands or heads, and the corresponding target orientation vectors  $\mathbf{o}_k$ , both hand and head orientation regression problems involve learning the mapping of color images  $\mathbf{C}_k$  onto the target orientations  $\mathbf{o}_k$ . For hands, the orientation vector  $\mathbf{o}_k = \{\phi_k, \psi_k\}^T \in \mathbb{R}^2$  contains Azimuth ( $\phi_k$ ) and Elevation ( $\psi_k$ ) angles, resulting from pronation/supination of the forearm and flexion/extension of the wrist, respectively [5]. Whereas head orientation is defined by yaw ( $\phi_k$ ), pitch ( $\psi_k$ ) and roll ( $\chi_k$ ) angles, i.e.  $\mathbf{o}_k = \{\phi_k, \psi_k, \chi_k\}^T \in \mathbb{R}^3$  [11]. We note that the problem of hand orientation regression is specifically challenging as there may be similar hand shapes in color images that map onto multiple orientations. We evaluate PROPEL's performance on the hand orientation dataset from [5], which contains 9414 images collected from 22 participants. For head

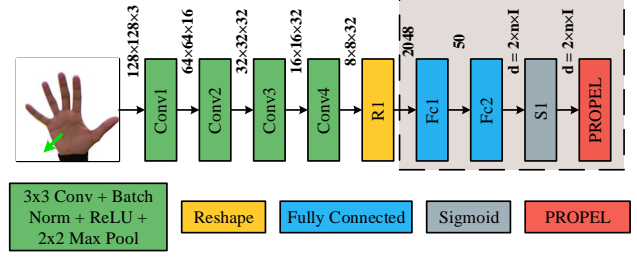


Figure 5: Flowchart shows the CNN regression architecture used for experimental validation of the proposed PROPEL loss (details in Section 4.1). The green arrow ( $\uparrow$ ) shows the target GT hand orientation that is only used during training. Scalar  $d$  represents the dimension of the network output. The comparison methods, described in Section 4.2, use the same overall architecture, where only the components in the highlighted box are replaced to match output dimensions required by a comparison loss function.

orientation, we evaluate the performance on publicly available BIWI dataset [11], which contains 10k images from 20 participants. The range of hand orientation angles captured by the hand orientation dataset are defined within a circular space with  $\sqrt{\phi^2 + \psi^2} \leq 45^\circ$ .

### 4.1. Network Architecture

The CNN network utilized for experimental validation of PROPEL is inspired from VGG networks [28] (Fig. 5). We keep the number of filters in each layer lower than in [28], as this does not have a significant impact on our model's performance to the orientation regression problems. For hand orientation regression, the input to our network is an RGB color image  $\mathbf{C}_k$  of size  $128 \times 128 \times 3$ , where the method learns to infer parameters for the model distribution in Equation 3. The maximum likelihood estimate (MLE) of the inferred parametric model distribution is used to get predicted hand orientation angles. The representation learning part of our network has four  $3 \times 3$  convolutional layers, where each layer is followed by batch normalization, a rectified non-linear unit (ReLU) and a  $2 \times 2$  max pooling layer. The output from the convolutional layers are resized and fed into two fully connected layers, Fc1 and Fc2 with 50 and  $d = 2 \times n \times I$  neurons, respectively. In our model distribution  $P_m$ , each dimension  $n$  requires two parameters, i.e. the mean and the variance of a Gaussian.  $P_m$  may have  $I$  Gaussians resulting in  $d = 2 \times n \times I$  parameters as output of Fc2.

The head orientation validation is done with the same network, however as the size of head images in BIWI dataset is small, the input image has size  $64 \times 64$ . We also modify Fc2 to enable inference of three-dimensional head orientation.

Table 1: Mean Absolute Error (MAE) in degrees along with number of model parameters for single-fold and 5-fold cross-validation.

Single-fold Validation				
Method	Azimuth ( $\phi$ )	Elevation ( $\psi$ )	CMAE	No. of Parameters
PROPEL (proposed)	<b>5.27°</b>	<b>3.99°</b>	<b>4.63</b>	126, 890
HEATMAP-MSE [13]	7.22°	6.07°	6.65	1, 248, 932
MSE	8.23°	7.18°	7.71	<b>126, 584</b>
SPORE [5]	8.49°	7.26°	7.88	-
MtR [4]	9.67°	7.97°	8.82	-
5-fold Cross-validation				
PROPEL (proposed)	<b>11.96°</b>	<b>10.00°</b>	<b>10.98</b>	126, 890
HEATMAP-MSE [13]	13.81°	10.42°	12.12	1, 248, 932
MSE	14.16°	11.51°	12.84	<b>126, 584</b>
SPORE [5]	15.73°	12.95°	14.34	-
MtR [4]	16.16°	12.83°	14.50	-

## 4.2. Comparison Methods

The proposed method is compared with existing state-of-the-art methods for hand orientation regression, namely, Marginalization through Regression (MtR) and Staged Probabilistic REgression (SPORE) [4, 5]. Both these methods employ hand-crafted features along with probabilistic learning frameworks for learning a multi-layered Random Forest regressor. We also compare PROPEL with two CNN regression loss methods, namely, Mean Squared Error (MSE) and probability heatmaps (HEATMAP-MSE). As PROPEL addresses probabilistic regression for a CNN, we compare it with the probability heatmap (HEATMAP-MSE) prediction framework inspired from [13, 31]. Following the methodology of [13, 31], the heatmap distributions for HEATMAP-MSE are generated by evaluating Equation 2 within a  $20 \times 20$  grid covering the domain  $\phi \in [-45^\circ, +45^\circ]$  and  $\psi \in [-45^\circ, +45^\circ]$ . Both MSE and HEATMAP-MSE use the same network architecture as PROPEL, except for the changes in the highlighted box in Fig. 5 to match the output dimensions of each comparison methods. MSE uses Fc2 with two neurons, whereas HEATMAP-MSE requires 500 neurons for Fc1 and 400 neurons for Fc2. The additional neurons are required to enable HEATMAP-MSE to learn  $20 \times 20 = 400$  dimensional target heatmap distributions. MSE and HEATMAP-MSE both use Mean Square Error as the loss function. A single-fold and 5-fold cross-validation is used to evaluate the performance of PROPEL in comparison to the hand orientation regression methods.

We also compare the performance of PROPEL on image-based head orientation regression task with existing literature. Performance of PROPEL is compared to existing CNN methods [20, 22] and a hand-crafted feature-based method [8]. [22] also utilizes synthetic data, however we only in-

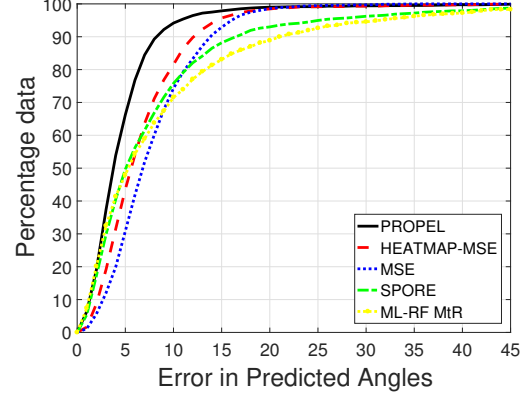


Figure 6: Percentage data versus prediction error shows the percentage data that lies below an error threshold for single-fold validation.

clude their results from real data for a fair comparison.

MSE and HEATMAP-MSE are independently trained for experimental validation. Both PROPEL and HEATMAP-MSE require additional ground truth (GT) variances to be defined in Equation 2. A large variance can over-smooth the GT PDF, producing underfitted prediction PDFs. However, a small variance yields a GT PDF that captures unwanted variations, resulting in overfitted model PDFs. We empirically found that a variance of  $(9^\circ)^2$ , for both Azimuth ( $\phi$ ) and Elevation ( $\psi$ ) angles, can optimally capture the variations within the dataset, while enabling both PROPEL and HEATMAP-MSE to generalize well. Additionally PROPEL also requires the number of Gaussians  $I$  in the model PDF  $P_m$ . We found that  $I = 2$  results in outperforming existing methods while showing the significance of having multiple components in  $P_m$ . Following the approach in [5], we utilize Mean Absolute Error (MAE) and Combined Mean Absolute Error (CMAE) for evaluating the overall performance of all comparison methods.

## 4.3. Experimental Validation for Hand Orientation Regression

We perform single-fold experimental evaluation by randomly dividing the dataset into training (70%), testing (20%) and validation (10%) sets. This evaluates the generalization performance of the comparison methods against a scenario where the training dataset is large enough to cover variations in hand shape, color, size and orientations. Additionally, we also evaluate the performance of our method using 5-fold cross-validation, where the folds are created by grouping multiple participants' data.

Table 1 shows Mean Absolute Error (MAE) along with the number of model parameters for CNN methods in the single-fold validation. We observe that the proposed PRO-

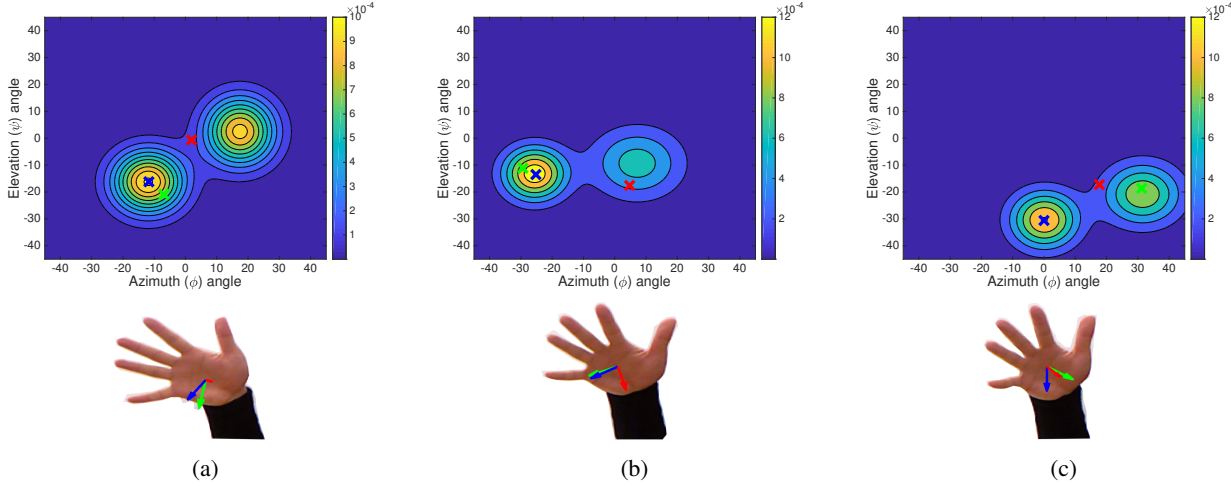


Figure 7: Ability of PROPEL to handle ambiguity in predictions, showing input hand images and the corresponding predicted PDFs from PROPEL. Hand orientation angles from GT (in green  $\uparrow \times$ ), and predictions from PROPEL (in blue  $\uparrow \times$ ) and MSE (in red  $\uparrow \times$ ) are shown. (a) - (b) show cases where PROPEL’s PDFs successfully handle ambiguities, whereas MSE predictions contain large error as they do not have ability to resolve ambiguities. (c) shows a case where PROPEL prediction contains a large error. We note that even in such case, the PDF contains useful information regarding the correct prediction.

PEL method outperforms existing state-of-the-art in both hand-crafted feature-based as well as CNN-based hand orientation regression. Probabilistic regression in both PROPEL and HEATMAP-MSE outperforms the widely used MSE loss. This is due to the ability of probabilistic methods to provide better generalization while addressing ambiguities in cases where multiple hand orientations can result in similar projected hand shape [5]. Furthermore, it can be observed from Table 1 that Azimuth ( $\phi$ ) angles have greater MAE as compared to Elevation ( $\psi$ ) angles for all comparison methods. This is due to the variations in inter-finger separation and styles for performing pronation/supination of the forearm across different participants in the hand orientation dataset. Fig. 6 provides further insight by showing the percentage of data that lies under a given error threshold for all comparison methods. We note that with PROPEL 95% of the data lies below  $10^\circ$  error, while HEATMAP-MSE has an error of  $15^\circ$  for the same percentage data. This demonstrates PROPEL’s ability to learn even with 10x fewer model parameters as compared to HEATMAP-MSE, while generalizing well using parametric probabilities.

In Fig. 7, we show some of the ambiguous cases and compare the probabilistic output from PROPEL against predictions from MSE. The PROPEL method has the ability to learn multiple hypotheses, due to the presence of multiple parameterized Gaussians in the model PDF. During training, the error is minimized for ambiguous targets where these Gaussians are able to model multiple hypotheses instead of being forced to a single hypothesis (as in MSE). On the other hand, MSE prediction *tries* to fit into the tar-

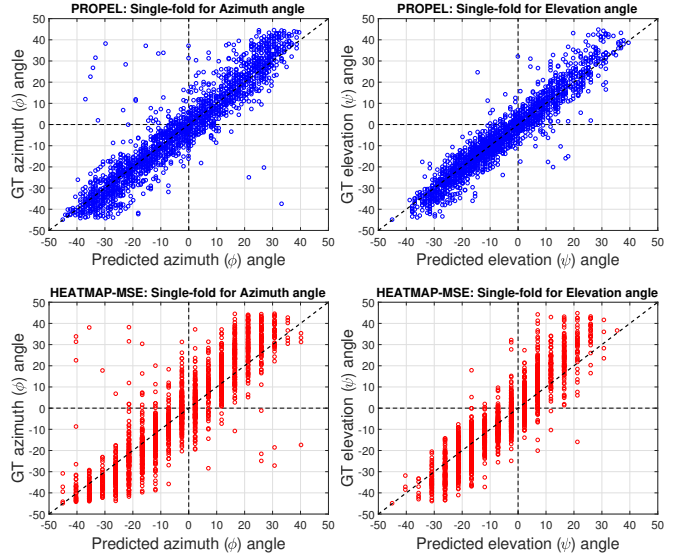


Figure 8: GT versus predicted angle plot using PROPEL (in blue  $\circ$ ) and HEATMAP-MSE (in red  $\circ$ ) shows Azimuth ( $\phi$ ) angles (left column) and Elevation ( $\psi$ ) angles (right column). A good regressor predicts angles close to GT angles, resulting in a diagonal line. PROPEL outperforms HEATMAP-MSE by accurately predicting angles, whereas the main source of error in HEATMAP-MSE is quantization due to  $20 \times 20$  heatmaps.

get space (see Fig 7 (a)-(b)). Fig. 7 (c) shows a failure case where PROPEL prediction results in a large error. We ob-



serve that even in such case, the predicted model PDF contains useful information regarding the correct prediction.

The most closely related method to PROPEL is HEATMAP-MSE as it also provides probabilistic regression by learning probability heatmaps. Table 1 and Fig. 8 show a comparison of these methods. We make two observations from this comparison. First, PROPEL uses approximately  $10\times$  fewer model parameters as compared to HEATMAP-MSE, while providing significantly better accuracy. This is due to the parametric probabilistic learning capability of PROPEL. Secondly, from Fig. 8 (second row), quantization due to  $20 \times 20$  heatmaps becomes the main source of errors in HEATMAP-MSE. Furthermore, it should be noted that with higher dimensional targets HEATMAP-MSE will require an exponentially larger number of model parameters, whereas our proposed PROPEL method will only result in increasing  $n$  which is linearly related by  $d = 2 \times n \times I$  to the model output parameters. Furthermore, unlike HEATMAP-MSE where predictions are constrained by the domain defined in heatmap distributions, PROPEL is capable of learning unconstrained target predictions without the need of heatmap distribution generation step.

The 5-fold cross-validation helps in understanding the generalization capability of each comparison method for inferring hand orientation for unseen participants' hand shape, color and size. Table 1 shows results from this experiment. PROPEL again outperforms all comparison methods by achieving least MAE. This experiment shows that utilizing the proposed PROPEL results in a CNN model that is able to generalize better than the existing state-of-the-art for CNN regression loss.

#### 4.4. Experimental Validation for Head Orientation Regression

For this comparison, we use the established experimental protocols from [20] and leave-one-out validation [8]. Table 2 shows comparison of PROPEL with existing state-of-the-art methods. Note that PROPEL is trained without any data augmentation, and the model is learned end-to-end unlike [20] that uses a pre-trained CNN. We did not run HEATMAP-MSE in this experiment as it becomes unwieldy in 3D, and BIWI requires estimation of three angles. In contrast, PROPEL can learn to infer probabilities for any higher dimensional target. PROPEL achieves competitive results with other methods and outperforms all techniques (including the state-of-the-art) in one of three angles, in both evaluation protocols. We also note, from Table 2, that PROPEL significantly reduces the model parameters, while achieving accuracy comparable to the state-of-the-art.

Table 2: MAE for experimental validation on BIWI dataset (\*indicates the use of evaluation protocol from [20])

Method	Pitch	Yaw	Roll	CMAE	No. of Parameters
<b>Unseen Faces (training=21 users and testing=3 users)*</b>					
PROPEL (proposed)	<b>3.44°</b>	4.02°	3.28°	<b>3.58°</b>	50, 294
MSE	9.20°	6.30°	5.15°	6.88°	<b>49, 835</b>
Lathuilière et al. [20]	4.68°	<b>3.12°</b>	<b>3.07°</b>	3.62°	135, 847, 232
Liu et al. [22]	6.10°	6.00°	5.94°	6.01°	595, 573
Drouard et al. [8]	5.43°	4.24°	4.13°	4.6°	-
<b>Unseen Faces (Leave-one-out validation)</b>					
PROPEL (proposed)	5.93°	5.81°	<b>4.53°</b>	5.42°	50, 294
MSE	7.70°	6.70°	5.81°	6.74°	<b>49, 835</b>
Liu et al. [22]	6.00°	6.10°	5.70°	<b>5.17°</b>	595, 573
Drouard et al. [8]	<b>5.90°</b>	<b>4.90°</b>	4.70°	5.93°	-

## 5. Conclusion

We proposed a novel PRObabilistic Parametric rEGression Loss (PROPEL) which enabled learning parametric probabilities for addressing regression problems using CNN. PROPEL is fully differentiable with an analytic closed-form solution to integrals, which allows it to be used with existing CNN architectures. A complete generalizable derivation for different level of complexity of prediction probabilities and multi-variate target dimensions was provided using Mixture of Gaussians. Comprehensive experimental validation showed that PROPEL outperforms previous state-of-the-art by a large margin. It shows better generalization capabilities while reducing the number of model parameters by a factor of 10. We also showed the usefulness of parametric probabilities for ambiguous cases where PROPEL handled prediction by providing multiple hypotheses. Our contribution can enable CNN regression models to have better prediction capabilities for addressing a range of problems. Our future work will explore the use of PROPEL in other challenging regression problems. We also aim to study the incorporation of other parametric probability distributions within PROPEL.

## References

- [1] B. Ahn, J. Park, and I. S. Kweon. Real-time head orientation from a monocular camera using deep neural network. In *Asian Conference on Computer Vision*, pages 82–96. Springer, 2014.
- [2] S. M. M. R. Al Arif, K. Knapp, and G. Slabaugh. Probabilistic spatial regression using a deep fully convolutional neural network. In *British Machine Vision Conference*. The British Machine Vision Association, 2017.
- [3] M. Asad and G. Slabaugh. Hand orientation regression using random forest for augmented reality. In *International Conference on Augmented and Virtual Reality*, 2014.
- [4] M. Asad and G. Slabaugh. Learning marginalization through regression for hand orientation inference. In *Computer Vision and Pattern Recognition (CVPR) Second Workshop on*

*Observing and Understanding Hands in Action (HANDS)*, 2016.

- [5] M. Asad and G. Slabaugh. Spore: Staged probabilistic regression for hand orientation inference. *Computer Vision and Image Understanding*, 2017.
- [6] C. M. Bishop. *Pattern recognition and machine learning*. springer, 2006.
- [7] A. Bulat and G. Tzimiropoulos. Human pose estimation via convolutional part heatmap regression. In *European Conference on Computer Vision*, pages 717–732. Springer, 2016.
- [8] V. Drouard et al. Head pose estimation via probabilistic high-dimensional regression. In *ICIP*, 2015.
- [9] J.-L. Durrieu et al. Lower and upper bounds for approximation of the kullback-leibler divergence between gaussian mixture models. In *ICASSP*, 2012.
- [10] D. Eigen, C. Puhrsch, and R. Fergus. Depth map prediction from a single image using a multi-scale deep network. In *Advances in neural information processing systems*, pages 2366–2374, 2014.
- [11] G. Fanelli, M. Dantone, J. Gall, A. Fossati, and L. Van Gool. Random forests for real time 3d face analysis. *International Journal of Computer Vision*, 101(3):437–458, 2013.
- [12] S. R. Fanello, C. Keskin, S. Izadi, P. Kohli, D. Kim, D. Sweeney, A. Criminisi, J. Shotton, S. B. Kang, and T. Paek. Learning to be a depth camera for close-range human capture and interaction. *ACM Transactions on Graphics (TOG)*, 33(4):86, 2014.
- [13] L. Ge, H. Liang, J. Yuan, and D. Thalmann. Robust 3d hand pose estimation in single depth images: from single-view cnn to multi-view cnns. In *Proceedings of the IEEE Conference on Computer Vision and Pattern Recognition*, pages 3593–3601, 2016.
- [14] R. Girshick, J. Donahue, T. Darrell, and J. Malik. Rich feature hierarchies for accurate object detection and semantic segmentation. In *Proceedings of the IEEE conference on computer vision and pattern recognition*, pages 580–587, 2014.
- [15] K. He, G. Gkioxari, P. Dollár, and R. Girshick. Mask r-cnn. *arXiv preprint arXiv:1703.06870*, 2017.
- [16] K. He, X. Zhang, S. Ren, and J. Sun. Deep residual learning for image recognition. In *Proceedings of the IEEE conference on computer vision and pattern recognition*, pages 770–778, 2016.
- [17] J. R. Hershey et al. Approximating the kullback leibler divergence between gaussian mixture models. In *ICASSP*, 2007.
- [18] C. Keskin, F. Kırac, Y. E. Kara, and L. Akarun. Hand pose estimation and hand shape classification using multi-layered randomized decision forests. In *European Conference on Computer Vision*, pages 852–863. Springer, 2012.
- [19] A. Krizhevsky, I. Sutskever, and G. E. Hinton. Imagenet classification with deep convolutional neural networks. In *Advances in neural information processing systems*, pages 1097–1105, 2012.
- [20] S. Lathuiliere, R. Juge, P. Mesejo, R. Munoz-Salinas, and R. Horaud. Deep mixture of linear inverse regressions applied to head-pose estimation. In *IEEE Conference on Computer Vision and Pattern Recognition*, volume 3, page 7, 2017.
- [21] Y. LeCun, Y. Bengio, and G. Hinton. Deep learning. *Nature*, 521(7553):436–444, 2015.
- [22] X. Liu, W. Liang, Y. Wang, S. Li, and M. Pei. 3d head pose estimation with convolutional neural network trained on synthetic images. In *Image Processing (ICIP), 2016 IEEE International Conference on*, pages 1289–1293. IEEE, 2016.
- [23] T. Narihira, M. Maire, and S. X. Yu. Direct intrinsics: Learning albedo-shading decomposition by convolutional regression. In *Proceedings of the IEEE International Conference on Computer Vision*, pages 2992–2992, 2015.
- [24] D. Pathak, P. Krähenbühl, S. X. Yu, and T. Darrell. Constrained structured regression with convolutional neural networks. *arXiv preprint arXiv:1511.07497*, 2015.
- [25] T. Pfister, J. Charles, and A. Zisserman. Flowing convnets for human pose estimation in videos. In *Proceedings of the IEEE International Conference on Computer Vision*, pages 1913–1921, 2015.
- [26] G. Sfikas, C. Constantinopoulos, A. Likas, and N. Galatsanos. An analytic distance metric for gaussian mixture models with application in image retrieval. *Artificial Neural Networks: Formal Models and Their Applications-ICANN 2005*, pages 755–755, 2005.
- [27] E. Shelhamer, J. Long, and T. Darrell. Fully convolutional networks for semantic segmentation. *IEEE transactions on pattern analysis and machine intelligence*, 39(4):640–651, 2017.
- [28] K. Simonyan and A. Zisserman. Very deep convolutional networks for large-scale image recognition. In *International Conference on Learning Representations*, 2015.
- [29] T. Tieleman and G. Hinton. Lecture 6.5-rmsprop: Divide the gradient by a running average of its recent magnitude. *COURSERA: Neural networks for machine learning*, 4(2):26–31, 2012.
- [30] J. Tompson, R. Goroshin, A. Jain, Y. LeCun, and C. Brengle. Efficient object localization using convolutional networks. In *Proceedings of the IEEE Conference on Computer Vision and Pattern Recognition*, pages 648–656, 2015.
- [31] J. Tompson, M. Stein, Y. Lecun, and K. Perlin. Real-time continuous pose recovery of human hands using convolutional networks. *ACM Transactions on Graphics (ToG)*, 33(5):169, 2014.
- [32] S. Zheng, S. Jayasumana, B. Romera-Paredes, V. Vineet, Z. Su, D. Du, C. Huang, and P. H. Torr. Conditional random fields as recurrent neural networks. In *Proceedings of the IEEE International Conference on Computer Vision*, pages 1529–1537, 2015.

## Appendix A. Derivation of Analytic Solution to Integrals

This section includes derivations of analytic solution to integrals for function  $G(\cdot)$  and  $H(\cdot)$  presented in the Section 3.2. Let  $\mathbf{x} = \{x_1, x_2, \dots, x_n\}^\top \in \mathbb{R}^n$  define the target prediction space with  $n$  dimensions. In order to facilitate analytic solution of our proposed loss function, we write the function  $G(P_i, P_j)$  between two Gaussian distributions  $P_i$  and  $P_j$  as:

$$G(P_i, P_j) = \int P_i P_j d\mathbf{x} = \int \dots \int P_i P_j dx_1 \dots dx_n, \quad (16)$$

$$= \int \dots \int \left[ \frac{e^{-\frac{1}{2} \left[ \frac{(x_1 - \mu_{x_{1i}})^2}{\sigma_{x_{1i}}} + \dots + \frac{(x_n - \mu_{x_{ni}})^2}{\sigma_{x_{ni}}} \right]}}{(\sqrt{2\pi})^n \sqrt{\sigma_{x_{1i}} \dots \sigma_{x_{ni}}}} \right] \left[ \frac{e^{-\frac{1}{2} \left[ \frac{(x_1 - \mu_{x_{1j}})^2}{\sigma_{x_{1j}}} + \dots + \frac{(x_n - \mu_{x_{nj}})^2}{\sigma_{x_{nj}}} \right]}}{(\sqrt{2\pi})^n \sqrt{\sigma_{x_{1j}} \dots \sigma_{x_{nj}}}} \right] dx_1 \dots dx_n, \quad (17)$$

$$= \int \dots \int \frac{e^{-\frac{1}{2} \left[ \frac{(x_1 - \mu_{x_{1i}})^2}{\sigma_{x_{1i}}} + \frac{(x_1 - \mu_{x_{1j}})^2}{\sigma_{x_{1j}}} + \dots + \frac{(x_n - \mu_{x_{ni}})^2}{\sigma_{x_{ni}}} + \frac{(x_n - \mu_{x_{nj}})^2}{\sigma_{x_{nj}}} \right]}}{(2\pi)^n \sqrt{(\sigma_{x_{1i}} \dots \sigma_{x_{ni}})(\sigma_{x_{1j}} \dots \sigma_{x_{nj}})}} dx_1 \dots dx_n, \quad (18)$$

$$= \int \dots \int \frac{e^{-\frac{1}{2} \left[ \frac{(x_1^2 - 2x_1\mu_{x_{1i}} + \mu_{x_{1i}}^2)\sigma_{x_{1j}} + (x_1^2 - 2x_1\mu_{x_{1j}} + \mu_{x_{1j}}^2)\sigma_{x_{1i}}}{\sigma_{x_{1i}}\sigma_{x_{1j}}} + \dots + \frac{(x_n - \mu_{x_{ni}})^2}{\sigma_{x_{ni}}} + \frac{(x_n - \mu_{x_{nj}})^2}{\sigma_{x_{nj}}} \right]}}{(2\pi)^n \sqrt{(\sigma_{x_{1i}} \dots \sigma_{x_{ni}})(\sigma_{x_{1j}} \dots \sigma_{x_{nj}})}} dx_1 \dots dx_n, \quad (19)$$

$$= \int \dots \int \frac{e^{\left[ -\frac{\sigma_{x_{1i}} + \sigma_{x_{1j}}}{2\sigma_{x_{1i}}\sigma_{x_{1j}}} x^2 + \frac{\mu_{x_{1i}}\sigma_{x_{1j}} + \mu_{x_{1j}}\sigma_{x_{1i}}}{\sigma_{x_{1i}}\sigma_{x_{1j}}} x - \frac{1}{2} \left[ \dots + \frac{\mu_{x_{1i}}^2\sigma_{x_{1j}} + \mu_{x_{1j}}^2\sigma_{x_{1i}}}{\sigma_{x_{1i}}\sigma_{x_{1j}}} + \frac{(x_n - \mu_{x_{ni}})^2}{\sigma_{x_{ni}}} + \frac{(x_n - \mu_{x_{nj}})^2}{\sigma_{x_{nj}}} \right] \right]}}{(2\pi)^n \sqrt{(\sigma_{x_{1i}} \dots \sigma_{x_{ni}})(\sigma_{x_{1j}} \dots \sigma_{x_{nj}})}} dx_1 \dots dx_n. \quad (20)$$

Given  $G(P_i, P_j)$ , we can now analytically evaluate the Gaussian for  $\int [\cdot] dx_1$  using the following theorem<sup>2</sup>:

$$\int_{-\infty}^{+\infty} e^{[-ax_1^2 + bx_1 - c]} dx_1 = e^{[\frac{b^2}{4a} - c]} \sqrt{\frac{\pi}{a}}. \quad (21)$$

We compare left hand side of Equation 21 with Equation 20 to determine  $a$ ,  $b$  and  $c$  as:

$$a = \frac{\sigma_{x_{1i}} + \sigma_{x_{1j}}}{2\sigma_{x_{1i}}\sigma_{x_{1j}}}, \quad (22)$$

$$b = \frac{\mu_{x_{1i}}\sigma_{x_{1j}} + \mu_{x_{1j}}\sigma_{x_{1i}}}{\sigma_{x_{1i}}\sigma_{x_{1j}}}, \quad (23)$$

$$c = \left[ \frac{\mu_{x_{1i}}^2\sigma_{x_{1j}} + \mu_{x_{1j}}^2\sigma_{x_{1i}}}{2\sigma_{x_{1i}}\sigma_{x_{1j}}} + \dots + \frac{(x_n - \mu_{x_{ni}})^2}{2\sigma_{x_{ni}}} + \frac{(x_n - \mu_{x_{nj}})^2}{2\sigma_{x_{nj}}} \right]. \quad (24)$$

Replacing  $a$ ,  $b$  and  $c$  in the right hand side of Equation 21 to get Equation:

$$G(P_i, P_j) = \int \dots \int \frac{e^{\left[ \frac{2\mu_{x_{1i}}\mu_{x_{1j}} - \mu_{x_{1i}}^2 - \mu_{x_{1j}}^2}{2(\sigma_{x_{1i}} + \sigma_{x_{1j}})} - \frac{1}{2} \left[ \frac{(x_2 - \mu_{x_{2i}})^2}{\sigma_{x_{2i}}} + \frac{(x_2 - \mu_{x_{2j}})^2}{\sigma_{x_{2j}}} + \dots + \frac{(x_n - \mu_{x_{ni}})^2}{\sigma_{x_{ni}}} + \frac{(x_n - \mu_{x_{nj}})^2}{\sigma_{x_{nj}}} \right] \right]}}{(2\pi)^{n-1} \sqrt{2\pi(\sigma_{x_{1i}} + \sigma_{x_{1j}})(\sigma_{x_{2i}}\sigma_{x_{2j}} \dots \sigma_{x_{ni}}\sigma_{x_{nj}})}} dx_2 \dots dx_n. \quad (25)$$

We can apply similar analytic solution for  $\int \dots \int [\cdot] dx_2 \dots dx_n$  to arrive at the Equation:

$$G(P_i, P_j) = \frac{e^{\left[ \frac{2\mu_{x_{1i}}\mu_{x_{1j}} - \mu_{x_{1i}}^2 - \mu_{x_{1j}}^2}{2(\sigma_{x_{1i}} + \sigma_{x_{1j}})} + \dots + \frac{2\mu_{x_{ni}}\mu_{x_{nj}} - \mu_{x_{ni}}^2 - \mu_{x_{nj}}^2}{2(\sigma_{x_{ni}} + \sigma_{x_{nj}})} \right]}}{(\sqrt{2\pi})^n \sqrt{(\sigma_{x_{1i}} + \sigma_{x_{1j}}) \dots (\sigma_{x_{ni}} + \sigma_{x_{nj}})}}. \quad (26)$$

<sup>2</sup>Gaussian Integral (accessed on 20-07-2018) <http://mathworld.wolfram.com/GaussianIntegral.html>

The second function we evaluate for helping our derivation is  $H(P_1)$  defined as:

$$H(P_i) = \int P_i^2 d\mathbf{x} = \int \cdots \int P_i^2 dx_1 \cdots dx_n, \quad (27)$$

$$= \int \cdots \int \left( \frac{e^{-\frac{1}{2} \left[ \frac{(x_1 - \mu_{x_{1i}})^2}{\sigma_{x_{1i}}} + \cdots + \frac{(x_n - \mu_{x_{ni}})^2}{\sigma_{x_{ni}}} \right]}}{(\sqrt{2\pi})^n \sqrt{\sigma_{x_{1i}} \cdots \sigma_{x_{ni}}}} \right)^2 dx_1 \cdots dx_n, \quad (28)$$

$$= \int \cdots \int \frac{e^{-\left[ \frac{(x_1 - \mu_{x_{1i}})^2}{\sigma_{x_{1i}}} + \cdots + \frac{(x_n - \mu_{x_{ni}})^2}{\sigma_{x_{ni}}} \right]}}{(2\pi)^n \sigma_{x_{1i}} \cdots \sigma_{x_{ni}}} dx_1 \cdots dx_n, \quad (29)$$

$$= \int \cdots \int \frac{e^{-\left[ \frac{x_1^2 - 2x_1\mu_{x_{1i}} + \mu_{x_{1i}}^2}{\sigma_{x_{1i}}} + \cdots + \frac{x_n^2 - 2x_n\mu_{x_{ni}} + \mu_{x_{ni}}^2}{\sigma_{x_{ni}}} \right]}}{(2\pi)^n \sigma_{x_{1i}} \cdots \sigma_{x_{ni}}} dx_1 \cdots dx_n. \quad (30)$$

Applying Equation 21, we reduce Equation 30 to:

$$H(P_i) = \frac{1}{(2\sqrt{\pi})^n \sqrt{\sigma_{x_{1i}} \cdots \sigma_{x_{ni}}}}. \quad (31)$$